A. Usseinov, Zh. Koishibayeva*, A. Akilbekov

L.N. Gumilyov Eurasian National University, Astana, Kazakhstan
E-mail: *zhanymgul.k@gmail.com

Hybrid DFT of electronic and vibrational properties of iron-doped B-GA$_2$O$_3$ crystals

Abstract. *This paper presents the results of calculations of energy and electron-optical properties of iron-doped β-Ga$_2$O$_3$. By analyzing the arrangement of the electronic levels of the impurity in the band gap for different charge states, it is shown that Fe is an acceptor impurity. Evaluation of both optical and thermodynamic transition levels indicates the deep nature of the iron acceptor impurity. In addition, iron can play the role of a donor at very low Fermi energies, but the probability of forming such a state is extremely low. We find that iron modifies Raman scattering in an ambiguous manner. Due to the low effective atomic mass of the substituted iron atom, doping leads to a pronounced enhancement of phonon modes of vibrations in the high-frequency range (~ 600÷800 cm^{-1}). The results obtained are in good agreement with experimental observations, confirming the acceptor character of the iron impurity.*
Keywords: *β-Ga$_2$O$_3$, optoelectronics, acceptor level, density functional theory.*

Introduction

Despite long history of research (more than 50 years), Ga$_2$O$_3$ crystals remain a well-studied material due to a wide range of potential applications [1-3]. Ga$_2$O$_3$ has five stable phases: α, β, γ, δ and ϵ [1]. Among them, the β phase is the most stable under thermodynamic equilibrium conditions, and therefore, widely studied. In many respects, scientific interest is supported by a suitable electronic structure of β-Ga$_2$O$_3$ and its wide band gap of 4.9 eV [4-7]. The latter makes the crystal transparent in the visible and near-UV spectrum. Due to this, β-Ga2O3 can be used in light emitting devices [8] and scintillation applications [9-11]. UV absorption with high photoresponse at the GaN/Sn:Ga2O3 p-n junction enables efficient UV photodetectors [9,12,13]. Meanwhile, the high breakdown field of β-Ga2O3 crystal (> 8MV/cm) allows its use in power devices: rectifiers and power metal-oxide-semiconductor field-effect transistors (MOSFETs) [14-16]. Finally, a recent study of Cr^{3+} doped α- and β-phase Ga2O3 showed good electronic flexibility for non-contact temperature measurements with suitable sensitivity and resolution [17]. All of these and further technological development as well as the adaptation of the knowledge gained to specific applications depend on a deep understanding of the evolution of electronic processes when impurities and intrinsic defects are introduced into a crystal through growth or irradiation processes [18,19].

It is known that controlled n-type conductivity is easily achievable in β-Ga2O3; however, reliable p-type conductivity has not yet been obtained [20, 21]. Meanwhile, efficient p-type conductivity opens up new opportunities for improving planar technologies in power electronics and optoelectronics. As is known, iron (Fe) and magnesium (Mg) are promising alloying additives for obtaining semi-insulating properties of Ga2O3 [22, 23]. Iron and magnesium act as deep acceptors and thereby compensate for n-type impurities. Fe-doped semi-insulating

16 | № 3(144)/2023

Л.Н. Гумилев атындағы ЕҰУ Хабаршысы. Физика. Астрономия сериясы
ISSN: 2616-6836, eISSN: 2663-1296

β-Ga2O3 crystals are commercially available and widely used as substrates for β-Ga2O3 epitaxial layers [24]. In these crystals, the concentration of Fe dopant is about 10^{18} cm^{-3} to compensate for background donors and pinning the Fermi level.

The deep donor-like level (E2) is measured as E$_c$-0.78 eV by transient deep-level spectroscopy and is attributed to Fe [25]. Another study using non-contact spectroscopy (DLTS) methods gives the Fe$^{2+/3+}$ charge transition level E$_c$ 0.84±0.05 eV [26]. Another work, using steady-state measurements of photoinduced electron paramagnetic resonance (EPR), identified an optically induced change in the charge state of Fe^{3+} with a level of 1.3±0.2 eV below the bottom of the conduction band [27]. However, it should be noted that the identification of experimentally determined values is limited only by the ionization process and cannot consider possible lattice interactions. In addition, measurements do not directly determine the type of impurity or type of internal defect involved in the transition.

When studying the red luminescence of Fe-doped crystals, Polyakov et.al. [28] reported two sharp emission lines near 1.78 eV and 1.80 eV at low temperatures, which suggests their origin from highly localized atomic states (for example, d-orbitals). They attributed the peak at 1.78 eV to the intracenter transition $^4T_1 - {}^6A_1$ Fe^{3+}. Another study by Sun et al. [29] suggests that these two sharp peaks at 688 nm and 696 nm are most likely due to Cr impurity based on polarized absorption results, luminescence observations, and analysis of Tanabe-Sugano diagrams.

Given the difficulties in interpreting the above experimental results, most of what we know about the properties has been derived from theory, especially density functional theory (DFT). For example, Yoshioka et al. [30] calculated lattice parameters, space groups, and volumetric expansion normalized to room temperature for various gallium oxide polymorphs. He et.al. [31] reported the structural parameters, band structure and Debye temperature of β-Ga2O3, also calculated based on density functional theory. Our recent DFT studies [32–34] correlate well with the abovementioned results. Additional results of calculations of physical properties and internal defects can be found in [22, 35–39].

This work aims to theoretically investigate the electronic structure of Fe-doped β-Ga2O3 by evaluating the calculated optical and thermodynamic bandgap impurity transition levels and analyzing the density of states and Raman scattering compared with experimentally observed data.

Methodology

2.1 Calculation details

All calculations were performed using the CRYSTAL-17 program [40] using the basis of linear combinations of atomic orbitals (LCAO). The all-electron Gaussian-type basis sets (BS) for gallium (Ga) and oxygen (O) atoms were taken from [41] and [42], respectively. We also used the basis from [43] for the iron (Fe) atom. We chose the nonlocal hybrid exchange-correlation functional B3PW [44] because it provides the best comparison of the structural and electronic properties of pure defect-free crystals with the results measured experimentally and described in the cited literature. The total energy convergence threshold for the self-consistent field (SCF) procedure was set to 10^{-7} and 10^{-8} a.u. for structural and frequency calculations, respectively. A quasi-Newtonian scheme has been used to optimize the geometry, which is implemented in the CRYSTAL17 code. The gradients are evaluated each time the total energy is calculated, and the second derivative matrix (i.e. the Hessian matrix) is built from the gradients and updated by the BFGS algorithm. Optimization is considered complete when the change in energy between iterations does not exceed 10^{-7} a.u. and conditions are achieved that satisfy the gradient and displacement criteria. The overall energy difference between the two SCF steps also has a high accuracy tolerance (10^{-7} a.u.). Effective atomic charges were calculated using Mulliken's population analysis [45]. Crystal reciprocal space integration was performed using a 4×4×4 Puck-Monchhorst grid, resulting in 30 k-points. The derivatives needed to construct the Hessian matrix were calculated numerically using the CRYSTAL17 code to calculate the frequencies of

ВЕСТНИК ЕНУ имени Л.Н. Гумилева. Серия Физика. Астрономия
BULLETIN of L.N. Gumilyov ENU. Physics. Astronomy Series

№ 3(144)/2023   17

the lattice vibrations at a point. [46,47]. Calculations of Raman tensors and spectral intensities were carried out using the coupled-perturbed Hartree–Fock approach [48].

To simulate the Fe-doped crystal, a periodic model of an extended unit cell (supercell) with a translation matrix of 1×4×2 along the axes and containing 160 atoms was used. After relaxation, the supercell parameters were a=12.29 Å, b=12.21 Å, c=11.65 Å, V=1699.6 Å3. The atomic concentration of Fe impurity is 1.56 in %, which is calculated as the ratio of the number of impurity atoms to the number of atoms in the Ga sublattice. Figure 1 shows the positions of Fe atoms in the regular positions of Ga atoms in the unit cell. Interstitial positions and substitutions at oxygen atom positions were not considered due to their high formation energy compared to Ga positions.
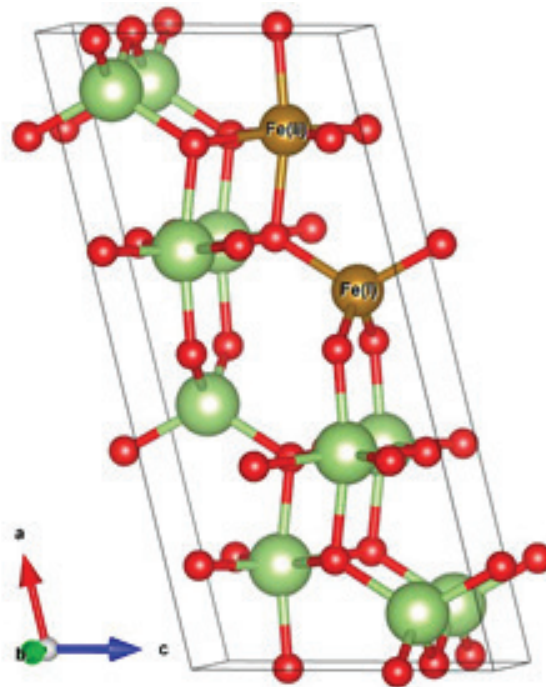
Figure 1. Fe atoms in substitution positions for Ga(I) and Ga(II) atoms.

2.2 Calculations of defect energy

The energy of formation of Fe in β-Ga2O3 is expressed as:

$$E_f\left(Fe_{Ga}^q\right) = E_{tot}\left(Fe_{Ga}^q\right) - E_{tot}(Ga_2O_3) + \mu(Ga) - \mu(Fe) + qE_F + E_{corr} \tag{1}$$

where $E_{tot}\left(Fe_{Ga}^q\right)$ — total energy of a Ga2O3 crystal with one substituting Fe_{Ga} in the charge state q, $E_{tot}(Ga_2O_3)$ – total energy of a pure Ga2O3 crystal. $\mu(Ga)$ and $\mu(Fe)$ — the chemical potentials of the Ga and Fe atoms, which varied between high and low oxygen chemical potentials, as will be described below. $q \times E_F$ is the change in electron energy due to the exchange of electrons and holes with the valence band. Finally, E_{corr} is a correction to the formation energy that takes into account the spurious electrostatic interaction between charged defects in neighboring supercells [49].

It is known that the energy of formation depends on the external conditions of crystal growth [50]. For example, the formation energy of an oxygen vacancy is determined by the relative abundance of Ga and O atoms, which are determined by the chemical potentials of the Ga and O atoms. At the same time, the chemical potential of the atoms depends on the experimental growth conditions. It varies within limits designated as high (O-rich) and low (Ga-rich) chemical potential. The state of the O_2 molecule is selected as the high chemical potential of oxygen, and

the metallic Ga is selected as the low chemical potential. Having made simple transformations from the following system of equations $\mu(O) < 1/2\mu(O_2) = 1/2E_{tot}(O_2)$; $\mu(Ga) < \mu(Ga^{metal}) = E_{tot}(Ga)$; $2\mu_{Ga}+3\mu_O=\mu(Ga_2O_3)=E_{tot}(Ga_2O_3)$ we obtain ranges of changes in chemical potentials. Chemical potential of oxygen:

$$1/3E_{tot}(Ga_2O_3) – 2/3E_{tot}(Ga) < \mu_O < 1/2\mu(O_2)$$

Similarly for the gallium potential:

$$1/2E_{tot}(Ga_2O_3) – 3/4E_{tot}(O_2) < \mu_{Ga} < \mu(Ga^{metal})$$

2.3 Transition levels

The transition level is defined as the Fermi level energy at which the formation energies of neutral and charged systems are equal [51,52]:

$$E_{tot}(D,q)\text{-}E_{tot}(bulk) + \sum_i n_i\mu_i + q\left(\varepsilon\left(\frac{q}{q}\right)\text{-}E_V\right) =$$
$$= E_{tot}(D,q') – E_{tot}(bulk) + \sum_i n_i\mu_i + q'(\varepsilon(q/q') – E_V) + E_{corr}$$

or

$$\varepsilon(q/q') = \frac{E_{tot}(D,q')-E_{tot}(D,q)-E_{corr}}{q-q'} + E_V \tag{2}$$

To simulate a negatively charged state, we add one electron to the system and, in the case of a positively charged state, one hole. The q' state always corresponds to a state with one more electron: $q' =q+1e$. Double charge transitions can be obtained from single charge transitions, for example: (+2/0) from (+1/0) and (+2/+1) as the average between them. The top of the valence band is set to zero energy, $E_V=0$.

Equation (2) can be used to calculate the optical transition levels $\varepsilon_{opt}(q/q')$, i.e. levels without taking into account the relaxation of the crystal lattice with a charged defect (adiabatic approximation). The thermodynamic levels are determined from the optical levels, taking into account the complete relaxation of the defective crystal structure, according to the following expression:

$$\varepsilon_{therm}\left(\frac{q}{q'}\right) = \varepsilon_{opt}\left(\frac{q}{q'}\right) \pm E_{rel} \tag{3}$$

where E_{rel} is the relaxation energy in absolute value, calculated based on the difference in total energies between the relaxed and unrelaxed charged system.

Results and discussion

3.1 Structural and electronic properties

As a result of the complete relaxation of the atomic structure with an iron impurity in the substitution positions of gallium atoms, the average distances between neighboring atoms near the iron atom, d(Fe-O), the effective charge and magnetic moment of the iron atom, as well as the change in the band gap in comparison with the pure crystal were calculated (see table 1). From the data obtained, it is clear that the charge of iron atoms is slightly higher than that of the gallium atoms in a pure crystal. This leads to a slight uncompensated charge in the lattice, which is reflected in a slight increase in bond lengths between the iron impurity and neighboring oxygen atoms. In addition, the increase in lattice parameters and bond lengths between the Fe ion and neighboring oxygens is due to the slightly larger ionic radius of iron compared to the gallium ion in the tetrahedral (0.47 vs 0.49 nm) and octahedral (0.062 vs 0.064 nm) positions

ВЕСТНИК ЕНУ имени Л.Н. Гумилева. Серия Физика. Астрономия
BULLETIN of L.N. Gumilyov ENU. Physics. Astronomy Series

№ 3(144)/2023   19

[53]. In general, all parameter values from Table 1 differ and depend on the position of Fe in the lattice. The latter indicates the anisotropy of the electronic structure of the crystal depending on the local environment. Thus, due to the higher coordination of iron in the octahedral position (Fe_{Ga2}), a slightly larger displacement of nearby atoms and a narrowing of the band gap are observed than for the tetrahedral position (Fe_{Ga1}). The obtained results are in excellent agreement with previously presented experimental data described in the literature [21, 25, 28, 54].

Figure 2 (a,b), the bottom of the conduction band is represented by empty 4s and unfilled 3d states of Fe (trap levels). In this case, iron ions can capture free electrons from the conduction band, effectively suppressing both unintended conduction and UV and blue luminescence. This conclusion is in excellent agreement with the experimental observation, namely, a significant decrease in free charge carriers and a transition to a semi-insulating state, as well as the disappearance of photoluminescence peaks [55, 56]. If Fe ions are positively charged (see Figures 2 c, d), new unoccupied Fe levels appear in the band gap, which lies much deeper at the level of ~2 eV and characterize the impurity as a deep donor. In the case of capturing an additional electron, the 3d level of the Fe impurity is filled and the Fermi level is shifted higher (see Figures 2 e, f). In this case, the remaining unoccupied states are characterized by empty 4s states of Fe, located at a height of 1 to 1.5 eV above the top of the valence band.

It is interesting to note the behavior of electronic states in the range from -8 to -5 eV. It can be seen that in the ground (neutral) state the levels of Fe and O overlap, forming a chemical bond. Positive ionization of Fe ions leads to an increase in the amplitude of 3d levels in the range -8 to -6 eV (see Figures 2 c, d), and negative ionization, on the contrary, leads to an increase in the amplitude of the states of O ions. This behavior indicates the appearance of additional attraction between impurity Fe ions with O ions in the case of positive ionization and repulsion in the case of negative ionization. Indeed, positive ionization leads to a decrease in the estimated Fe-O bond length by approximately ~0.1 Å, to 1.78 Å (in tetrahedral coordination (Fe_{Ga1}) and up to 1.94 Å in octahedral coordination (Fe_{Ga2}) compared to the neutral state (see Table 1) On the contrary, with negative ionization, the oxygen environment around Fe moves away due to additional electrostatic repulsion. For the tetrahedral disposition, the bond length is 1.97 Å, and for the octahedral disposition is 2.12 Å.

Table 1. Calculated average distance between Fe and O ions, d(Fe-O), effective charge q, magnetic moment μ(Fe), and band gap E_g

	d(Fe-O),Å	q, e	μ(Fe), μ_B	E_g, eV
Ga_2O_3-Fe(I)	1.87	+1.71	4.21	4.81
Ga_2O_3-Fe(II)	2.03	+1.72	4.33	4.73
Ga_2O_3	1.85/2.0	+1.68/–1.1	–	4.89
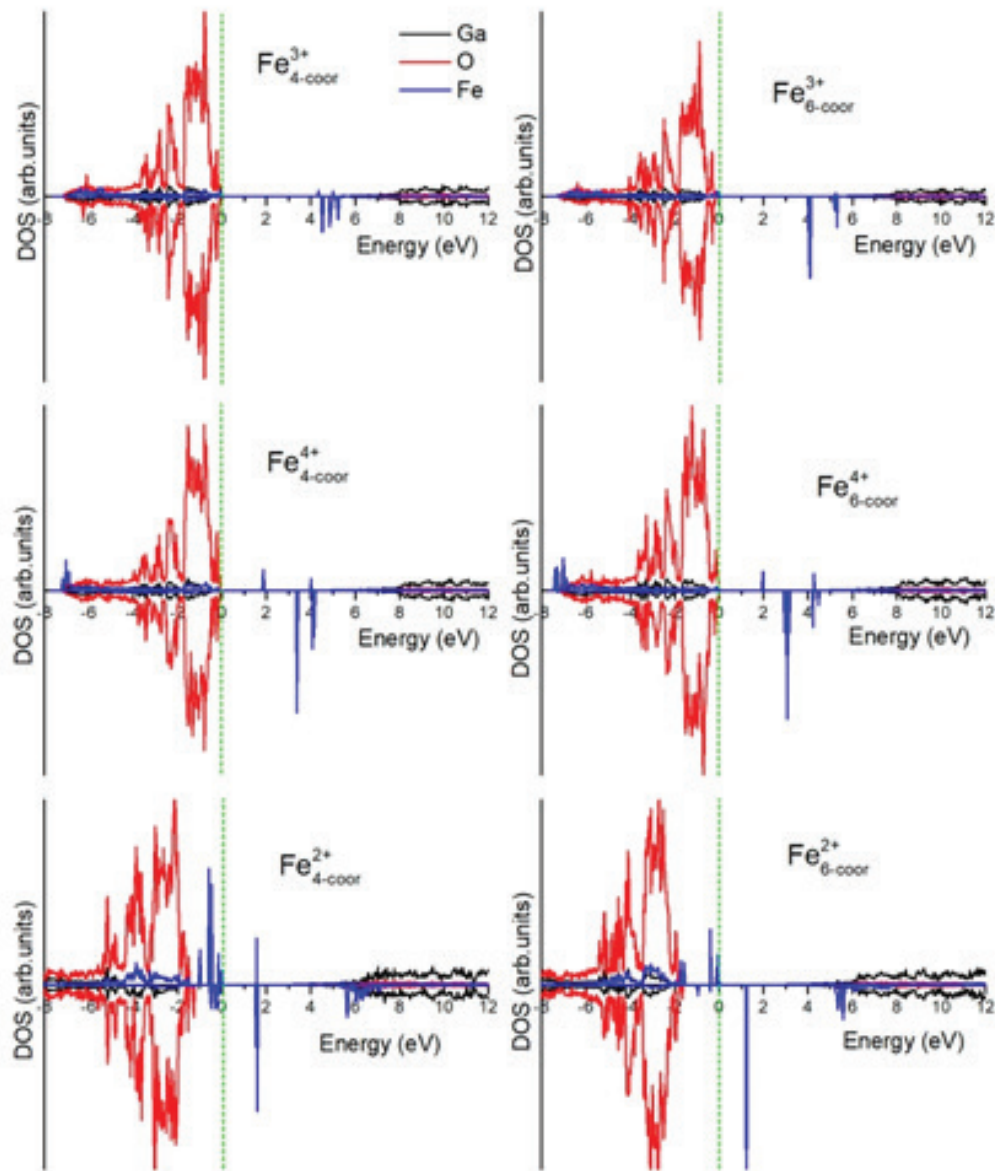
Figure 1. Total density of states for Fe$_{Ga1}$ (a,c,e) and Fe$_{Ga2}$ (b,d,f) in β-Ga2O3. All impurity states have been magnified by factor 5. Green-dashed-vertical lines represent the Fermi level.

3.2 Transition levels

A deep acceptor character of Fe in β-Ga2O3 has been well established and confirmed by a number of experimental evidence and first-principles calculations. For instance, using deep level transient spectroscopy (DLTS), secondary ion mass spectrometry (SIMS), and first-principles calculations, it has been found that Fe impurity is responsible for the trap level around 0.8 eV below the bottom of conduction band [25]. At this, intrinsic defects, such as V$_{Ga}$, V$_{O}$, and related defects, were assigned to another close-spaced level of 0.75 eV, which is observed in samples irradiated with 600 keV protons at room temperature [57]. In another study, the change in the Fermi level has been calculated from UV photoemission spectra (UPS) [54]. The Fermi level decreases from 3.94 to 3.78 eV after annealing of iron-doped crystals, which may be due to the capture of excited electrons from the conduction band by Fe^{3+} traps, indicating that the trap depth may be more than 1 eV. Using the hybrid screened HSE functional, the thermodynamic levels were predicted to be located at a depth of 0.59 and 0.61 eV for Fe$_{Ga1}$ and Fe$_{Ga2}$, respectively [25].

ВЕСТНИК ЕНУ имени Л.Н. Гумилева. Серия Физика. Астрономия
BULLETIN of L.N. Gumilyov ENU. Physics. Astronomy Series

№ 3(144)/2023   21

It has also been shown that β-Ga2O3 doped with ~400 ppm iron exhibits a higher conductivity photoresponse under excitation of 4.4–4.8 eV. This indicates that Fe has a deep donor level above the top of the valence band [58].

To quantitatively confirm these considerations, we have calculated the optical and thermodynamic transition levels of iron. We've found that the accumulation of iron impurity in the Ga(2) site is favored due to the slightly lower formation energy compared to the Ga(1) site, although both sites are energetically favorable. Under conditions of high chemical potential of gallium atoms, the energy of iron formation increases by ~1 eV (see Figure 2a). During the negative iron ionization, when transition from a neutral to negatively charged (-1) state occurs, the corresponding levels of the optical transition $\varepsilon_{opt}(0/-1)$ lie at a depth of more than 1 eV from the bottom of the conduction band, which indicates the deep acceptor nature of iron. At the same time, positive ionization of iron reveals the presence of a deep donor transition level $\varepsilon_{opt}(1+/0)$, which lies deep 4 eV below the bottom of the conduction band or 1 eV above the top of the valence band.

We have also calculated the thermodynamic transition levels corresponding to the thermal excitation energies of deep or shallow donor (acceptor) centers. In contrast to the optical transition level, it assumes complete relaxation of the charged defect structure. As can be seen from Table 2, $\varepsilon_{therm}(0/-1)$ shifts towards the center of the band gap, indicating deeper trap levels lying more than 2 eV below the bottom of the conduction band. $\varepsilon_{therm}(1+/0)$ has the same tendency with a shift of levels by 1.8 eV above the top of the valence band. Overall, our results strongly suggest that iron is a deep acceptor and is in good agreement with previous theoretical studies and experimental findings.
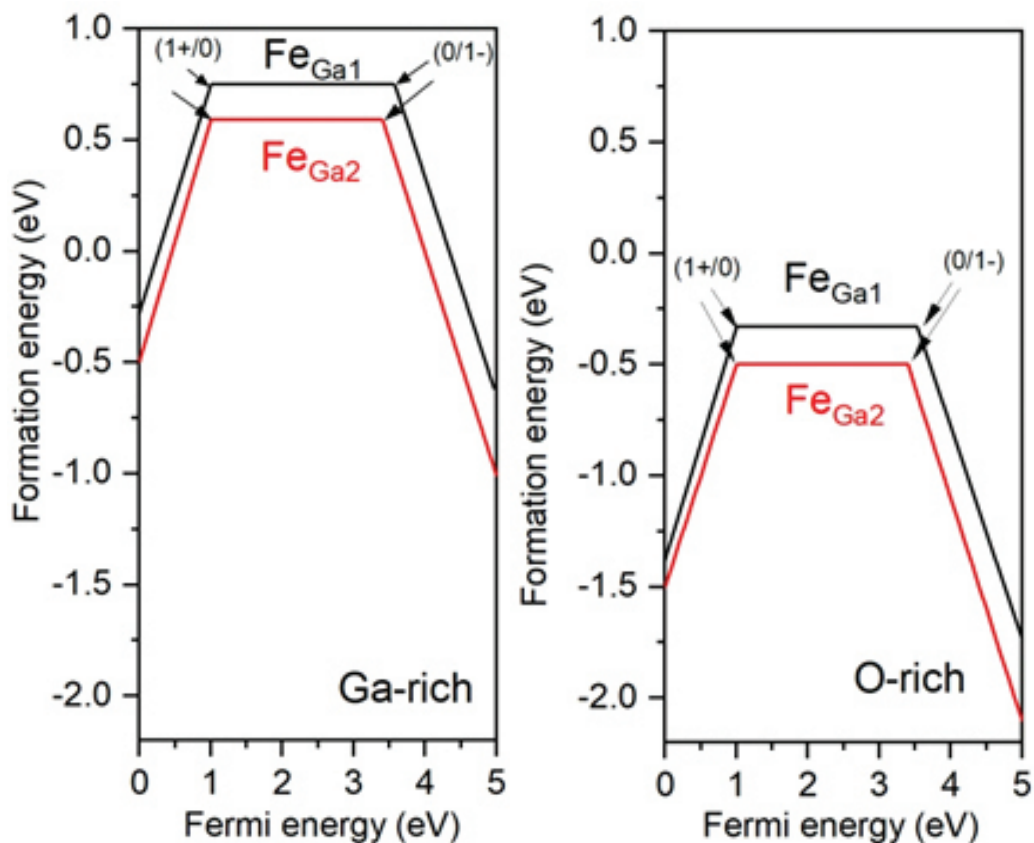
Figure 2. Formation energies for Fe substituted Ga positions in *β*-Ga2O3 plotted against the Fermi energy for Ga-rich (a) and O-rich conditions (b).

Table 2. Transition levels ε(q/q') (in eV) for an iron-doped β-Ga2O3 crystal

	Transition levels	ε_{opt}	ε_{therm}	E_{rel}
Fe$_{Ga1}$	1+/0	1.0	1.8	0.8
	0/–1	3.6	2.36	1.24
Fe$_{Ga2}$	1+/0	1.0	1.7	0.7
	0/–1	3.5	2.77	0.73

3.3 Raman spectra

The results of the calculation of the Raman spectra are shown in Figure 3. Eleven peaks have been detected for all samples. These peaks observed at 125, 157, 178, 207, 322, 350, 460, 494, 622, 662, and 761 cm^{-1} correspond to Bg(2), Ag(2), Ag(3), Ag(4), Ag(5), Ag(6), Ag(7) Ag(8), Ag(9), and Ag(10) phonon modes, respectively. As a rule, the low-frequency zone (I) at 125, 157, 178, 207 cm^{-1} is associated with vibration and translation of tetrahedral and octahedral chains, the mid-frequency zone (II) at 322, 350, 460, 494 cm^{-1} reflects the deformation of the GaO6 octahedron, and high-frequency zones (III) and (IV) at 622, 662 and 761 cm^{-1} relate to the stretching and bending of the GaO4 tetrahedron [59,60]. The experimentally observed Raman spectra of β-Ga2O3 [54] show peaks at 115, 146, 171, 201, 321, 348, 418, 477, 632, 660, and 768 cm^{-1} (indicated by red arrows in Figure 3), which are in good agreement with the calculated peaks. Good agreement between the calculated and experimental spectra means the high quality of the synthesized crystals. Considering the supposed shortcomings of the calculation model and the fact that the real material defects cannot be isolated, the experimental spectra are generally consistent with the calculated spectra for pure β-Ga2O3.
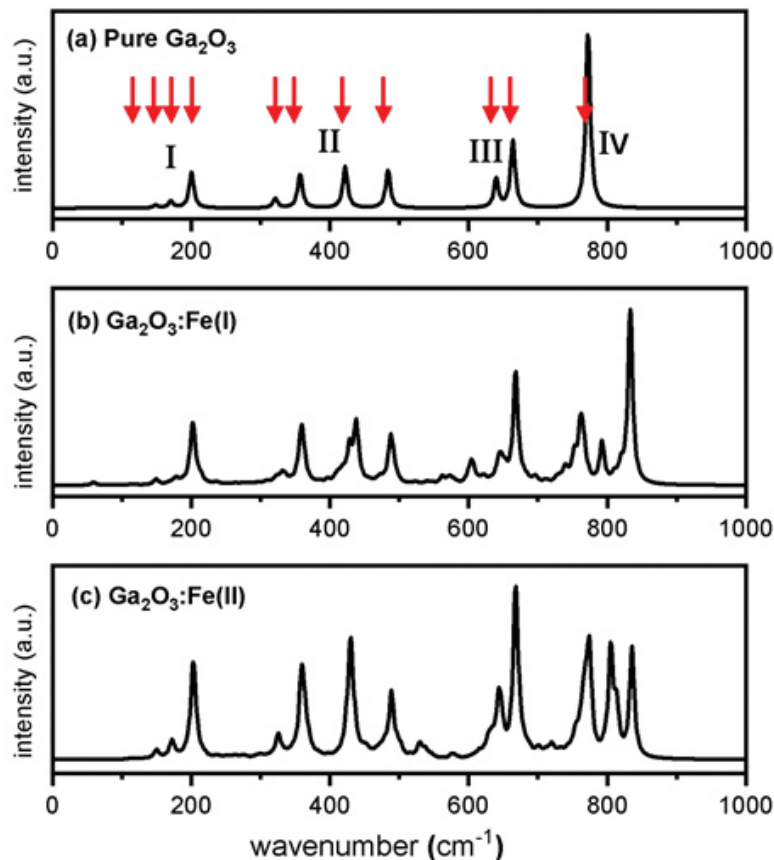
Figure 3. Calculated full Raman spectra for pure Ga2O3 (a),
Fe$_{Ga1}$:Ga2O3 (b) and Fe$_{Ga2}$:Ga2O3 (c)

ВЕСТНИК ЕНУ имени Л.Н. Гумилёва. Серия Физика. Астрономия
BULLETIN of L.N. Gumilyov ENU. Physics. Astronomy Series

№ 3(144)/2023   23

Doping with iron led to an ambiguous change in the spectrum. In general, for Fe(1) and Fe(2), a small change is observed in low-frequency modes, which may be due to two competing mechanisms: 1) a decrease in mode intensity due to an increase in lattice parameters due to the slightly larger Fe atom size; and 2) mode enhancement due to a decrease in effective atomic mass. The average frequency range for Fe(1) has not changed significantly, while for Fe(2) an additional peak appears at 529 cm^{-1}, indicating an increase in the contribution of GaO6 to the deformation. In the high-frequency range, a slight positive peak shift compared to the pure crystal is observed for both Fe positions and a relative increase in intensity. The mode at 761 cm^{-1} after Fe doping decayed into 3, which the enhancement of the vibrational component of tetrahedra and octahedra can explain. As already has been noted, the latter may be due to the low effective atomic mass of the substituting Fe atom, which dominates the slight increase in bond length. This ultimately leads to an increase in the frequency of vibrational modes in the high-frequency range.

Conclusions

This paper presents the results of a hybrid B3PW study of the electronic structure of Fe-doped β-Ga2O3 by evaluating the calculated optical and thermodynamic band gap impurity transition levels, as well as analyzing the density of states and Raman spectra in comparison with experimentally observed data.

We have found that Fe leads to a slight increase in lattice parameters at the expense of a slightly larger ionic radius. Electronic state analysis has showed that Fe ions can capture free electrons from the conduction band, effectively suppressing both unintended conduction and UV-visible luminescence. Positive ionization of Fe ions leads to an increase in the amplitude of 3d levels from -8 to -6 eV (see Figure 1 c, d), and negative ionization, on the contrary, leads to an increase in the amplitude of the O ion state.

We have found that Fe has a dual nature; it has deep donor and deep acceptor levels. However, the deep acceptor nature of Fe is preferred because the donor state has a higher formation energy.

The calculated Raman scattering of pure β-Ga2O3 agrees well with the observed one. Doping with Fe led to an ambiguous change in the spectrum; however, the overall picture of the spectrum is preserved due to insignificant relaxations after the introduction of Fe. For the Fe impurity, changes are observed mainly in the high-frequency region, which indicates an increase in the vibrational modes of tetrahedral and octahedral bonds.

References

1. Pearton S.J. et al. A review of Ga_2O_3 materials, processing, and devices // Appl. Phys. Rev. – 2018. – T. 5. № 1. – C. 011301.

2. Zhang J. et al. Recent progress on the electronic structure, defect, and doping properties of Ga_2O_3 // APL Mater. AIP Publishing LLCAIP Publishing – 2020. – T. 8. № 2. – C. 020906.

3. Stepanov S.I. et al. Gallium oxide: Properties and applications - A review // Rev. Adv. Mater. Sci. – 2016. – T. 44. № 1. – C. 63-86.

4. He H. et al. First-principles study of the structural, electronic, and optical properties of Ga_2O_3 in its monoclinic and hexagonal phases // Phys. Rev. B - Condens. Matter Mater. Phys. - 2006. T. 74. № 19. – C. 1-8.

5. Janowitz C. et al. Experimental electronic structure of In_2O_3 and Ga_2O_3 // New J. Phys. IOP Publishing – 2011. –T. 13. № 8. –C. 085014.

6. Sasaki K. et al. Ga_2O_3 schottky barrier diodes fabricated by using single-crystal β-Ga_2O_3 (010) substrates // IEEE Electron Device Lett. – 2013. –T. 34. № 4. – C. 493-495.

7. Konishi K. et al. 1-kV vertical Ga_2O_3 field-plated Schottky barrier diodes // Appl. Phys. Lett. AIP Publishing LLC AIP Publishing – 2017. –T. 110. № 10. –C. 103506.

8. Galazka Z. β-Ga_2O_3 for wide-bandgap electronics and optoelectronics // Semicond. Sci. Technol. IOP Publishing – 2018. – T. 33. № 11. – C. 113001.

9. Luchechko A. et al. Luminescence spectroscopy of Cr^{3+} ions in bulk single crystalline β-Ga_2O_3 // J. Phys. D. Appl. Phys. IOP Publishing. – 2020. –Т. 53. № 35. – C. 354001.

10. Usui Y. et al. Ce-doped Ga_2O_3 single crystalline semiconductor showing scintillation features // Optik (Stuttg). Elsevier GmbH. – 2017. –Т.143. –С. 150-157.

11. Drozdowski W. et al. β-Ga_2O_3:Ce as a fast scintillator: An unclear role of cerium // Radiat. Meas. – 2019. – Т. 121. – C. 49-53.

12. Li W. et al. Fabrication of cerium-doped β-Ga_2O_3 epitaxial thin films and deep ultraviolet photodetectors // Appl. Opt. – 2018. – Т. 57. № 3. – C. 538.

13. Alhalaili B. et al. Gallium oxide nanowires for UV detection with enhanced growth and material properties // Sci. Reports 2020 101. Nature Publishing Group. – 2020. – Т. 10. № 1. – C. 1-14.

14. Kresse G., Furthmüller J. Efficient iterative schemes for *ab initio* total-energy calculations using a plane-wave basis set // Phys. Rev. B. American Physical Society. – 1996. – Т. 54. № 16. – C. 11169.

15. Varley J.B., Schleife A. Bethe–Salpeter calculation of optical-absorption spectra of In_2O_3 and Ga_2O_3 // Semicond. Sci. Technol. IOP Publishing. – 2015. – Т. 30. № 2. – C. 024010.

16. Tadjer M.J. et al. Editors' Choice Communication—A (001) β-Ga_2O_3 MOSFET with +2.9 V Threshold Voltage and HfO_2 Gate Dielectric // ECS J. Solid State Sci. Technol. IOP Publishing. – 2016. – Т. 5. № 9. – C. P468.

17. Back M. et al. Boltzmann Thermometry in Cr^{3+}-Doped Ga_2O_3 Polymorphs: The Structure Matters // Adv. Opt. Mater. – 2021. – Т. 9. № 9. – C. 2100033.

18. Ai W. et al. Radiation damage in β-Ga_2O_3 induced by swift heavy ions // Jpn. J. Appl. Phys. IOP Publishing. – 2019. – Т. 58. № 12. – C. 120914.

19. Farzana E. et al. Impact of deep level defects induced by high energy neutron radiation in β-Ga_2O_3 // APL Mater. – 2019. – Т. 7. № 2. – C. 022502.

20. Baldini M., Galazka Z., Wagner G. Recent progress in the growth of β-Ga_2O_3 for power electronics applications // Mater. Sci. Semicond. Process. Elsevier Ltd. – 2018. – Т. 78. № July. – C. 132-146.

21. Lyons J.L. A survey of acceptor dopants for β-Ga_2O_3 // Semicond. Sci. Technol. IOP Publishing. – 2018. – Т. 33. № 5. – C. 05LT02.

22. McCluskey M.D. Point defects in Ga_2O_3 // J. Appl. Phys. – 2020. – Т. 127. – C. 101101.

23. Peelaers H., Van de Walle C.G. Brillouin zone and band structure of β-Ga_2O_3 // Phys. status solidi. John Wiley & Sons, Ltd. – 2015. – Т. 252. № 4. – C. 828–832.

24. Sun C. et al. Fabrication of β-Ga_2O_3 thin films and solar-blind photodetectors by laser MBE technology // Opt. Mater. Express. Optical Society of America. – 2014. – Т. 4. № 5. – C. 1067-1076.

25. Ingebrigtsen M.E. et al. Iron and intrinsic deep level states in Ga_2O_3 // Appl. Phys. Lett. AIP Publishing LLC AIP Publishing. – 2018. – Т. 112. № 4. – C. 042104.

26. Lenyk C.A. et al. Deep donors and acceptors in β-Ga_2O_3 crystals: Determination of the $Fe^{2+/3+}$ level by a noncontact method // J. Appl. Phys. American Institute of Physics Inc. – 2019. – Т. 126. № 24.

27. Bhandari S., Zvanut M.E., Varley J.B. Optical absorption of Fe in doped Ga_2O_3 // J. Appl. Phys. American Institute of Physics Inc. – 2019. – Т. 126. № 16. – C. 165703.

28. Polyakov A.Y. et al. Electrical Properties, Deep Levels and Luminescence Related to Fe in Bulk Semi-Insulating β-Ga_2O_3 Doped with Fe // ECS J. Solid State Sci. Technol. The Electrochemical Society. – 2019. – Т. 8. № 7. – C. Q3091–Q3096.

29. Sun R. et al. On the origin of red luminescence from iron-doped β-Ga_2O_3 bulk crystals // Appl. Phys. Lett. American Institute of Physics Inc. – 2020. – Т. 117. № 5. – C. 52101.

30. Yoshioka S. et al. Structures and energetics of Ga_2O_3 polymorphs // J. Phys. Condens. Matter. IOP Publishing. – 2007. – Т. 19. № 34. – C. 346211.

31. He H., Blanco M.A., Pandey R. Electronic and thermodynamic properties β-Ga_2O_3 // Appl. Phys. Lett. American Institute of PhysicsAIP. – 2006. – Т. 88. № 26. – C. 261904.

32. Usseinov A. et al. Ab-Initio Calculations of Oxygen Vacancy in Ga_2O_3 Crystals // Latv. J. Phys. Tech. Sci. Sciendo. – 2021. – Т. 58. № 2. – C. 3-10.

33. Usseinov A. et al. Vacancy Defects in Ga_2O_3: First-Principles Calculations of Electronic Structure // Materials (Basel). Multidisciplinary Digital Publishing Institute. – 2021. – Т. 14. № 23. – C. 7384.

34. Usseinov A. et al. Pair vacancy defects in β-Ga_2O_3 crystal: Ab initio study // Opt. Mater. X. Elsevier. – 2022. – Т. 16. – C. 100200.

35. Lee S.D., Akaiwa K., Fujita S. Thermal stability of single crystalline alpha gallium oxide films on sapphire substrates // Phys. status solidi. John Wiley & Sons, Ltd. – 2013. – Т. 10. № 11. – C. 1592-1595.

ВЕСТНИК ЕНУ имени Л.Н. Гумилева. Серия Физика. Астрономия
BULLETIN of L.N. Gumilyov ENU. Physics. Astronomy Series

№ 3(144)/2023   25

36. Poncé S., Giustino F. Structural, electronic, elastic, power, and transport properties of β-Ga_2O_3 from first principles // Phys. Rev. Res. American Physical Society. – 2020. – Т. 2. № 3. – С. 033102.

37. Kyrtsos A., Matsubara M., Bellotti E. Migration mechanisms and diffusion barriers of vacancies in Ga_2O_3 // Phys. Rev. B. American Physical Society. – 2017. – Т. 95. № 24. – С. 245202.

38. Blanco M.A. et al. Energetics and migration of point defects in Ga_2O_3 // Phys. Rev. B - Condens. Matter Mater. Phys. American Physical Society. 2005. – Т. 72. № 18. – С. 184103.

39. Peelaers H. et al. Deep acceptors and their diffusion in Ga_2O_3 // APL Mater. American Institute of Physics Inc. – 2019. – Т. 7. № 2.

40. Dovesi R. et al. Quantum-mechanical condensed matter simulations with CRYSTAL // Wiley Interdiscip. Rev. Comput. Mol. Sci. John Wiley & Sons, Ltd. – 2018. – Т. 8. № 4. – С. e1360.

41. Pandey R., Jaffe J.E., Harrison N.M. Ab initio study of high pressure phase transition in GaN // J. Phys. Chem. Solids. – 1994. – Т. 55. № 11. – С. 1357-1361.

42. Towler M.D. et al. Ab initio study of MnO and NiO // Phys. Rev. B. American Physical Society. – 1994. – Т. 50. № 8. – С. 5041-5054.

43. Vilela Oliveira D. et al. BSSE-correction scheme for consistent gaussian basis sets of double- and triple-zeta valence with polarization quality for solid-state calculations // J. Comput. Chem. John Wiley & Sons, Ltd. – 2019. – Т. 40. № 27. – С. 2364-2376.

44. Becke A.D. Density-functional thermochemistry. III. The role of exact exchange // J. Chem. Phys. – 1993. – Т. 98. № 7. – С. 5648-5652.

45. Mulliken R.S. Electronic population analysis on LCAO-MO molecular wave functions. II. Overlap populations, bond orders, and covalent bond energies // J. Chem. Phys. - 1955. – Т. 23. № 10. – С. 1841-1846.

46. Pascale F. et al. The calculation of the vibrational frequencies of crystalline compounds and its implementation in the CRYSTAL code // J. Comput. Chem. John Wiley & Sons, Ltd. - 2004. – Т. 25. № 6. – С. 888-897.

47. Zicovich-Wilson C.M. et al. Calculation of the vibration frequencies of α-quartz: The effect of Hamiltonian and basis set // J. Comput. Chem. John Wiley & Sons, Ltd. - 2004. – Т. 25. № 15. – С. 1873-1881.

48. Ferrero M. et al. Coupled perturbed Hartree-Fock for periodic systems: The role of symmetry and related computational aspects // J. Chem. Phys. AIP Publishing. - 2008. – Т. 128. № 1.

49. Makov G., Payne M.C. Periodic boundary conditions in ab initio calculations // Phys. Rev. B. - 1995. – Т. 51. № 7. – С. 4014-4022.

50. Van De Walle C.G., Neugebauer J. First-principles calculations for defects and impurities: Applications to III-nitrides // J. Appl. Phys. - 2004. – Т. 95. № 8. – С. 3851-3879.

51. Lany S., Zunger A. Assessment of correction methods for the band-gap problem and for finite-size effects in supercell defect calculations: Case studies for ZnO and GaAs // Phys. Rev. B - Condens. Matter Mater. Phys. - 2008. – Т. 78. № 23. – С. 235104.

52. Scherz U., Scheffler M. Density-Functional Theory of sp-Bonded Defects in III/V Semiconductors // Semicond. Semimetals. Elsevier. - 1993. – Т. 38. № С. – С. 1-58.

53. Kittel C. Introduction to Solid State Physics. 8th ed. New York: Wiley. - 2004. 704 с.

54. Zhang N. et al. Structural and electronic characteristics of Fe-doped β-Ga_2O_3 single crystals and the annealing effects // J. Mater. Sci. 2021 5623. Springer. - 2021. – Т. 56. № 23. – С. 13178-13189.

55. Harwig T., Kellendonk F. Some observations on the photoluminescence of doped β-galliumsesquioxide // J. Solid State Chem. – 1978. – Т. 24. № 3–4. – С. 255-263.

56. Harwig T., Wubs G.J., Dirksen G.J. Electrical properties of β-Ga_2O_3 single crystals // Solid State Commun. Pergamon. – 1976. – Т. 18. № 9–10. – С. 1223-1225.

57. Ingebrigtsen M.E. et al. Impact of proton irradiation on conductivity and deep level defects in β-Ga_2O_3 // APL Mater. American Institute of Physics Inc. - 2019. – Т. 7. № 2.

58. Irmscher K. et al. Electrical properties of β-Ga_2O_3 single crystals grown by the Czochralski method // J. Appl. Phys. AIP Publishing. - 2011. – Т. 110. № 6.

59. Galván C. et al. Structural and Raman studies of Ga_2O_3 obtained on GaAs substrate // Mater. Sci. Semicond. Process. Pergamon. – 2016. – Т. 41. – С. 513-518.

60. Onuma T. et al. Polarized Raman spectra in β-Ga_2O_3 single crystals // J. Cryst. Growth. North-Holland. – 2014. – Т. 401. – С. 330-333.

А.Б. Усеинов, Ж.К. Койшыбаева, А.Т. Акилбеков

Л.Н. Гумилев атындағы Еуразия ұлттық университеті, Астана, Қазақстан

Темір қосылған β-Ga$_2$O$_3$ кристалының электронды және дірілдік қасиеттерінің гибридті DFT

Аңдатпа. Бұл жұмыста темір қосылған β-Ga$_2$O$_3$ энергетикалық және электронды-оптикалық қасиеттерін есептеу нәтижелері келтірілген.Әр түрлі зарядтау күйлері үшін тыйым салынған аймақтағы электронды қоспа деңгейлерінің орналасуын талдау арқылы Fe акцепторлық қоспа екені анықталды. Оптикалық және термодинамикалық өтпелі деңгейлерді бағалау темірдің акцепторлық қоспасының терең сипатын көрсетеді. Сонымен қатар, темір Ферми энергиясының өте төмен мәндерінде донор рөлін атқара алады, алайда мұндай жағдайдың пайда болу ықтималдығы өте аз. Біз темір қоспасының комбинациялық шашырауды екіұшты түрде өзгертетінін анықтадық. Алмастыратын темір атомының төмен тиімді атомдық массасына байланысты допинг жоғары жиілікті диапазондағы тербелістердің фонондық режимдерінің айқын жоғарылауына әкеледі (~600÷800 см$^{-1}$). Нәтижелер темір қоспасының акцепторлық сипатын растайтын эксперименттік бақылаулармен жақсы үйлеседі.

Түйін сөздер: β-Ga$_2$O$_3$, оптоэлектроника, акцепторлық деңгей, тығыздық функциясының теориясы.

А.Б. Усеинов, Ж.К. Койшыбаева, А.Т. Акилбеков

Евразийский национальный университет им. Л.Н. Гумилева, Астана, Казахстан

Гибридные DFT электронных и вибрационных свойств кристалла β-Ga$_2$O$_3$ допированных железом

Аннотация. В данной работе представлены результаты расчетов энергетических и электронно-оптических свойств β-Ga2O3, легированного железом. Анализируя расположение уровней электронных примесей в запрещенной зоне для различных состояний заряда, показано, что Fe является акцепторной примесью. Оценка как оптических, так и термодинамических уровней перехода указывает на глубокую природу акцепторной примеси железа. Кроме того, железо может играть роль донора при очень низких энергиях Ферми, но вероятность образования такого состояния крайне мала. Мы обнаружили, что железо неоднозначно изменяет комбинационное рассеяние света. Из-за низкой эффективной атомной массы замещающего атома железа легирование приводит к выраженному усилению фононных мод колебаний в высокочастотном диапазоне (~600÷800 см$^{-1}$). Полученные результаты хорошо согласуются с экспериментальными наблюдениями, подтверждающими акцепторную природу примеси железа.

Ключевые слова: β-Ga$_2$O$_3$, оптоэлектроника, уровень акцептора, теория функционала плотности.

References

1. Pearton S.J. et al. A review of Ga$_2$O$_3$ materials, processing, and devices // Appl. Phys. Rev. 2018. - Vol. 5, № 1.P. 011301.

2. Zhang J. et al. Recent progress on the electronic structure, defect, and doping properties of Ga$_2$O$_3$ // APL Mater. AIP Publishing LLCAIP Publishing, 2020. Vol. 8, № 2. P. 020906.

3. Stepanov S.I. et al. Gallium oxide: Properties and applications - A review // Rev. Adv. Mater. Sci. 2016. Vol. 44, № 1. P. 63-86.

4. He H. et al. First-principles study of the structural, electronic, and optical properties of Ga$_2$O$_3$ in its monoclinic and hexagonal phases // Phys. Rev. B - Condens. Matter Mater. Phys. 2006. Vol. 74, № 19. P. 1-8.

5. Janowitz C. et al. Experimental electronic structure of In$_2$O$_3$ and Ga$_2$O$_3$ // New J. Phys. IOP Publishing, 2011. Vol. 13, № 8. P. 085014.

ВЕСТНИК ЕНУ имени Л.Н. Гумилева. Серия Физика. Астрономия
BULLETIN of L.N. Gumilyov ENU. Physics. Astronomy Series

№ 3(144)/2023

27

6. Sasaki K. et al. Ga_2O_3 schottky barrier diodes fabricated by using single-crystal β-Ga_2O_3 (010) substrates // IEEE Electron Device Lett. 2013. Vol. 34, № 4. P. 493-495.

7. Konishi K. et al. 1-kV vertical Ga_2O_3 field-plated Schottky barrier diodes // Appl. Phys. Lett. AIP Publishing LLC AIP Publishing , 2017. Vol. 110, № 10. P. 103506.

8. Galazka Z. β-Ga_2O_3 for wide-bandgap electronics and optoelectronics // Semicond. Sci. Technol. IOP Publishing, 2018. Vol. 33, № 11. P. 113001.

9. Luchechko A. et al. Luminescence spectroscopy of Cr^{3+} ions in bulk single crystalline β-Ga_2O_3 // J. Phys. D. Appl. Phys. IOP Publishing, 2020. Vol. 53, № 35. P. 354001.

10. Usui Y. et al. Ce-doped Ga_2O_3 single crystalline semiconductor showing scintillation features // Optik (Stuttg). Elsevier GmbH., 2017. Vol. 143. P. 150-157.

11. Drozdowski W. et al. β-Ga_2O_3:Ce as a fast scintillator: An unclear role of cerium // Radiat. Meas. 2019. Vol. 121, № October 2018. P. 49-53.

12. Li W. et al. Fabrication of cerium-doped β-Ga_2O_3 epitaxial thin films and deep ultraviolet photodetectors // Appl. Opt. 2018. Vol. 57, № 3. P. 538.

13. Alhalaili B. et al. Gallium oxide nanowires for UV detection with enhanced growth and material properties // Sci. Reports 2020 101. Nature Publishing Group, 2020. Vol. 10, № 1. P. 1-14.

14. Kresse G., Furthmüller J. Efficient iterative schemes for *ab initio* total-energy calculations using a plane-wave basis set // Phys. Rev. B. American Physical Society, 1996. Vol. 54, № 16. P. 11169.

15. Varley J.B., Schleife A. Bethe–Salpeter calculation of optical-absorption spectra of In_2O_3 and Ga_2O_3 // Semicond. Sci. Technol. IOP Publishing, 2015. Vol. 30, № 2. P. 024010.

16. Tadjer M.J. et al. Editors' Choice Communication— A (001) β-Ga_2O_3 MOSFET with +2.9 V Threshold Voltage and HfO_2 Gate Dielectric // ECS J. Solid State Sci. Technol. IOP Publishing, 2016. Vol. 5, № 9. P. P468.

17. Back M. et al. Boltzmann Thermometry in Cr^{3+}-Doped Ga_2O_3 Polymorphs: The Structure Matters! // Adv. Opt. Mater. 2021. Vol. 9, № 9. P. 2100033.

18. Ai W. et al. Radiation damage in β-Ga_2O_3 induced by swift heavy ions // Jpn. J. Appl. Phys. IOP Publishing, 2019. Vol. 58, № 12. P. 120914.

19. Farzana E. et al. Impact of deep level defects induced by high energy neutron radiation in β-Ga_2O_3 // APL Mater. 2019. Vol. 7, № 2. P. 022502.

20. Baldini M., Galazka Z., Wagner G. Recent progress in the growth of β-Ga_2O_3 for power electronics applications // Mater. Sci. Semicond. Process. Elsevier Ltd, 2018. Vol. 78, № July. P. 132-146.

21. Lyons J.L. A survey of acceptor dopants for β-Ga_2O_3 // Semicond. Sci. Technol. IOP Publishing, 2018. Vol. 33, № 5. P. 05LT02.

22. McCluskey M.D. Point defects in Ga_2O_3 // J. Appl. Phys. 2020. Vol. 127. P. 101101.

23. Peelaers H., Van de Walle C.G. Brillouin zone and band structure of β-Ga_2O_3 // Phys. status solidi. John Wiley & Sons, Ltd, 2015. Vol. 252, № 4. P. 828-832.

24. Sun C. et al. Fabrication of β-Ga_2O_3 thin films and solar-blind photodetectors by laser MBE technology // Opt. Mater. Express. Optical Society of America, 2014. Vol. 4, № 5. P. 1067-1076.

25. Ingebrigtsen M.E. et al. Iron and intrinsic deep level states in Ga_2O_3 // Appl. Phys. Lett. AIP Publishing LLC AIP Publishing, 2018. Vol. 112, № 4. P. 042104.

26. Lenyk C.A. et al. Deep donors and acceptors in β-Ga_2O_3 crystals: Determination of the $Fe^{2+/3+}$ level by a noncontact method // J. Appl. Phys. American Institute of Physics Inc., 2019. Vol. 126, № 24.

27. Bhandari S., Zvanut M.E., Varley J.B. Optical absorption of Fe in doped Ga_2O_3 // J. Appl. Phys. American Institute of Physics Inc., 2019. Vol. 126, № 16. P. 165703.

28. Polyakov A.Y. et al. Electrical Properties, Deep Levels and Luminescence Related to Fe in Bulk Semi-Insulating β-Ga_2O_3 Doped with Fe // ECS J. Solid State Sci. Technol. The Electrochemical Society, 2019. Vol. 8, № 7. P. Q3091-Q3096.

29. Sun R. et al. On the origin of red luminescence from iron-doped β-Ga_2O_3 bulk crystals // Appl. Phys. Lett. American Institute of Physics Inc., 2020. Vol. 117, № 5. P. 52101.

30. Yoshioka S. et al. Structures and energetics of Ga_2O_3 polymorphs // J. Phys. Condens. Matter. IOP Publishing, 2007. Vol. 19, № 34. P. 346211.

31. He H., Blanco M.A., Pandey R. Electronic and thermodynamic properties β-Ga_2O_3 // Appl. Phys. Lett. American Institute of PhysicsAIP, 2006. Vol. 88, № 26. P. 261904.

32. Usseinov A. et al. Ab-Initio Calculations of Oxygen Vacancy in Ga_2O_3 Crystals // Latv. J. Phys. Tech. Sci. Sciendo, 2021. Vol. 58, № 2. P. 3-10.

33. Usseinov A. et al. Vacancy Defects in Ga_2O_3: First-Principles Calculations of Electronic Structure // Materials (Basel). Multidisciplinary Digital Publishing Institute, 2021. Vol. 14, № 23. P. 7384.

28   № 3(144)/2023

Л.Н. Гумилев атындағы ЕҰУ Хабаршысы. Физика. Астрономия сериясы
ISSN: 2616-6836, eISSN: 2663-1296

34. Usseinov A. et al. Pair vacancy defects in β-Ga$_2$O$_3$ crystal: Ab initio study // Opt. Mater. X. Elsevier, 2022. Vol. 16. P. 100200.

35. Lee S.D., Akaiwa K., Fujita S. Thermal stability of single crystalline alpha gallium oxide films on sapphire substrates // Phys. status solidi. John Wiley & Sons, Ltd, 2013. Vol. 10, № 11. P. 1592-1595.

36. Poncé S., Giustino F. Structural, electronic, elastic, power, and transport properties of β-Ga$_2$O$_3$ from first principles // Phys. Rev. Res. American Physical Society, 2020. Vol. 2, № 3. P. 033102.

37. Kyrtsos A., Matsubara M., Bellotti E. Migration mechanisms and diffusion barriers of vacancies in Ga$_2$O$_3$ // Phys. Rev. B. American Physical Society, 2017. Vol. 95, № 24. P. 245202.

38. Blanco M.A. et al. Energetics and migration of point defects in Ga$_2$O$_3$ // Phys. Rev. B - Condens. Matter Mater. Phys. American Physical Society, 2005. Vol. 72, № 18. P. 184103.

39. Peelaers H. et al. Deep acceptors and their diffusion in Ga$_2$O$_3$ // APL Mater. American Institute of Physics Inc., 2019. Vol. 7, № 2.

40. Dovesi R. et al. Quantum-mechanical condensed matter simulations with CRYSTAL // Wiley Interdiscip. Rev. Comput. Mol. Sci. John Wiley & Sons, Ltd, 2018. Vol. 8, № 4. P. e1360.

41. Pandey R., Jaffe J.E., Harrison N.M. Ab initio study of high pressure phase transition in GaN // J. Phys. Chem. Solids. 1994. Vol. 55, № 11. P. 1357-1361.

42. Towler M.D. et al. Ab initio study of MnO and NiO // Phys. Rev. B. American Physical Society, 1994. Vol. 50, № 8. P. 5041–5054.

43. Vilela Oliveira D. et al. BSSE-correction scheme for consistent gaussian basis sets of double- and triple-zeta valence with polarization quality for solid-state calculations // J. Comput. Chem. John Wiley & Sons, Ltd, 2019. Vol. 40, № 27. P. 2364-2376.

44. Becke A.D. Density-functional thermochemistry. III. The role of exact exchange // J. Chem. Phys. 1993. Vol. 98, № 7. P. 5648-5652.

45. Mulliken R.S. Electronic population analysis on LCAO-MO molecular wave functions. II. Overlap populations, bond orders, and covalent bond energies // J. Chem. Phys. 1955. Vol. 23, № 10. P. 1841-1846.

46. Pascale F. et al. The calculation of the vibrational frequencies of crystalline compounds and its implementation in the CRYSTAL code // J. Comput. Chem. John Wiley & Sons, Ltd, 2004. Vol. 25, № 6. P. 888-897.

47. Zicovich-Wilson C.M. et al. Calculation of the vibration frequencies of α-quartz: The effect of Hamiltonian and basis set // J. Comput. Chem. John Wiley & Sons, Ltd, 2004. Vol. 25, № 15. P. 1873-1881.

48. Ferrero M. et al. Coupled perturbed Hartree-Fock for periodic systems: The role of symmetry and related computational aspects // J. Chem. Phys. AIP Publishing, 2008. Vol. 128, № 1.

49. Makov G., Payne M.C. Periodic boundary conditions in ab initio calculations // Phys. Rev. B. 1995. Vol. 51, № 7. P. 4014-4022.

50. Van De Walle C.G., Neugebauer J. First-principles calculations for defects and impurities: Applications to III-nitrides // J. Appl. Phys. 2004. Vol. 95, № 8. P. 3851-3879.

51. Lany S., Zunger A. Assessment of correction methods for the band-gap problem and for finite-size effects in supercell defect calculations: Case studies for ZnO and GaAs // Phys. Rev. B - Condens. Matter Mater. Phys. 2008. Vol. 78, № 23. P. 235104.

52. Scherz U., Scheffler M. Density-Functional Theory of sp-Bonded Defects in III/V Semiconductors // Semicond. Semimetals. Elsevier, 1993. Vol. 38, № C. P. 1-58.

53. Kittel C. Introduction to Solid State Physics. 8th ed. New York: Wiley, 2004. 704 p.

54. Zhang N. et al. Structural and electronic characteristics of Fe-doped β-Ga$_2$O$_3$ single crystals and the annealing effects // J. Mater. Sci. 2021 5623. Springer, 2021. Vol. 56, № 23. P. 13178-13189.

55. Harwig T., Kellendonk F. Some observations on the photoluminescence of doped β-galliumsesquioxide // J. Solid State Chem. 1978. Vol. 24, № 3–4. P. 255-263.

56. Harwig T., Wubs G.J., Dirksen G.J. Electrical properties of β-Ga$_2$O$_3$ single crystals // Solid State Commun. Pergamon, 1976. Vol. 18, № 9–10. P. 1223-1225.

57. Ingebrigtsen M.E. et al. Impact of proton irradiation on conductivity and deep level defects in β-Ga$_2$O$_3$ // APL Mater. American Institute of Physics Inc., 2019. Vol. 7, № 2.

58. Irmscher K. et al. Electrical properties of β-Ga$_2$O$_3$ single crystals grown by the Czochralski method // J. Appl. Phys. AIP Publishing, 2011. Vol. 110, № 6.

59. Galván C. et al. Structural and Raman studies of Ga$_2$O$_3$ obtained on GaAs substrate // Mater. Sci. Semicond. Process. Pergamon, 2016. Vol. 41. P. 513-518.

60. Onuma T. et al. Polarized Raman spectra in β-Ga$_2$O$_3$ single crystals // J. Cryst. Growth. North-Holland, 2014. Vol. 401. P. 330-333.

ВЕСТНИК ЕНУ имени Л.Н. Гумилева. Серия Физика. Астрономия
BULLETIN of L.N. Gumilyov ENU. Physics. Astronomy Series

№ 3(144)/2023   29

Сведения об авторах:

A. Usseinov – PhD, Associate Professor, L.N.Gumilyov Eurasian National University, 2 Satpayev str., Astana, Kazakhstan.

Zh. Koishybayeva – Master's student, L.N.Gumilyov Eurasian National University, 2 Satpayev str., Astana, Kazakhstan.

A. Akilbekov – Doctor of Physical and Mathematical Sciences, Professor, L.N.Gumilyov Eurasian National University, 2 Satpayev str., Astana, Kazakhstan.

А.Б. Усеинов – PhD, доцент, Л.Н. Гумилев атындағы Евразия Ұлттық университеті, Сатпаев көш., 2, Астана қ., Қазақстан.

Ж.К. Койшыбаева – магистрант, Л.Н. Гумилев атындағы Евразия Ұлттық университеті, Сатпаев көш., 2, Астана қ., Қазақстан.

А.Т. Акилбеков – ф.-м.ғ.д., профессор, Л.Н. Гумилев атындағы Евразия Ұлттық университеті, Сатпаев көш., 2, Астана қ., Қазақстан.

А.Б. Усеинов – PhD, доцент, Евразийский национальный университет, ул. Сатпаева, 2, Астана, Казахстан.

Ж.К. Койшыбаева – магистрант, Евразийский национальный университет, ул. Сатпаева, 2, Астана, Казахстан.

А.Т. Акилбеков – д.ф.-м.н., профессор, Евразийский национальный университет, ул. Сатпаева, 2, Астана, Казахстан.

30 № 3(144)/2023

Л.Н. Гумилев атындағы ЕҰУ Хабаршысы. Физика. Астрономия сериясы
ISSN: 2616-6836, eISSN: 2663-1296